

Geophysical Research Letters

RESEARCH LETTER

10.1029/2021GL092815

Key Points:

- There is no simple relationship between cross-correlation coefficient (CC) and interevent separation
- CC is affected by many factors and thus lacks the resolution to determine two events as true repeating or just neighboring earthquakes
- To reliably identify repeating earthquakes, we should rely on the precise estimation of both source dimension and interevent distance

Supporting Information:

Supporting Information may be found in the online version of this article.

Correspondence to:

H. Kao,
honn.kao@canada.ca

Citation:

Gao, D., Kao, H., & Wang, B. (2021). Misconception of waveform similarity in the identification of repeating earthquakes. *Geophysical Research Letters*, 48, e2021GL092815. <https://doi.org/10.1029/2021GL092815>

Received 2 FEB 2021

Accepted 31 MAY 2021

Misconception of Waveform Similarity in the Identification of Repeating Earthquakes

Dawei Gao^{1,2} , Honn Kao^{1,2} , and Bei Wang^{1,2}

¹School of Earth and Ocean Sciences, University of Victoria, Victoria, BC, Canada, ²Pacific Geoscience Centre, Geological Survey of Canada, Sidney, BC, Canada

Abstract Identification of repeating earthquakes (repeaters) usually depends on waveform similarity expressed as the corresponding cross-correlation coefficient (CC) above a prescribed threshold, typically ranging in 0.70–0.98. However, the robustness and effectiveness of such a strategy have rarely been fully examined. In this study, we examine whether CC is a valid proxy for repeater identification through both synthetic and real earthquake experiments. We reveal that CC is controlled by not only the interevent distance but also many other factors, including station azimuth, epicentral distance, and velocity structure. Consequently, CC lacks the resolution in identifying true repeaters. For reliable repeater identification, we should consider the interevent overlap. Specifically, we define an event pair to be true repeaters if their interevent separation is smaller than the source dimension of the larger event. Our results imply that a systematic recheck of previously identified repeaters and associated interpretations/hypotheses may be important and necessary.

Plain Language Summary Repeating earthquakes (repeaters) are events that occur repeatedly on the same fault patch with the same fault directional motion and similar amount of slip. They provide important insights into a variety of geophysical subjects such as fault behavior, subsurface structure change, inner core rotation, and nucleation process of earthquakes and landslides. The identification of repeaters is usually solely based on waveform similarity, but the criteria can vary significantly from one case to another. With both synthetic and real data, we find that waveform similarity is controlled by many factors, in addition to interevent distance. Therefore, higher degree of waveform similarity does not necessarily imply a smaller hypocenter separation, and vice versa. Our results undoubtedly suggest that waveform similarity alone is insufficient for repeater identification. To more reliably identify repeaters, we should rely on the overlap of the source areas. Quantitatively, we define a repeating pair if their interevent distance is smaller than the rupture area of the larger event. Our results imply that previously identified repeaters and associated interpretations/hypotheses may be unreliable and hence need a systematic reexamination.

1. Introduction

Repeating earthquakes (repeaters) are events that recurrently rupture the same fault patch with the same focal mechanisms, often characterized by nearly identical waveforms (Abercrombie et al., 2020; Gao & Kao, 2020; Hatch et al., 2020; Sheng et al., 2021; Uchida & Bürgmann, 2019). These events are of great importance in many aspects of geophysics, such as monitoring subtle temporal changes of crustal properties (e.g., Pacheco et al., 2017; Poupinet et al., 1984; Sawazaki et al., 2015; Schaff & Beroza, 2004) and oceanic temperature (Wu et al., 2020), estimating fault creep (e.g., Materna et al., 2018; Matsubara et al., 2005; Nadeau & Johnson, 1998; Uchida et al., 2003, 2006; Yu, 2013), investigating inner core rotation (e.g., A. Li & Richards, 2003; Tkalčić et al., 2013; Zhang et al., 2005, 2008), evaluating the precision of earthquake locations (e.g., Jiang et al., 2014; A. Li & Richards, 2003; Meier et al., 2004; Schaff & Richards, 2011), and providing insights into the nucleation process of earthquakes (Huang & Meng, 2018; Kato & Nakagawa, 2014; Kato et al., 2012; Meng et al., 2015) and landslides (Yamada et al., 2016).

There are three ways of identifying repeaters. The most straightforward approach is by considering the overlap of the source areas (e.g., Waldhauser & Ellsworth, 2002). However, this physics-based approach requires a dense near-source array to precisely estimate the interevent distance and source dimension. The second, and perhaps the most popular way, relies on waveform similarity between an event pair (~64% in Table S1).

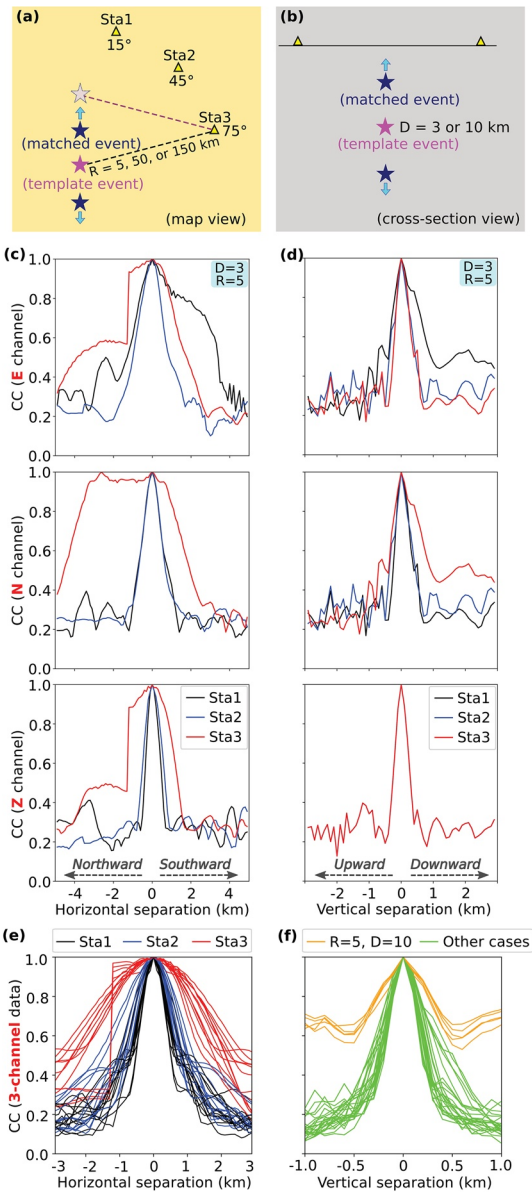


Figure 1. Synthetic experiment setup (a, b) and results showing CC variation as a function of horizontal (c, e) and vertical (d, f) interevent separation. (a) For horizontal interevent separation, the template event (fuchsia star) is fixed in the middle while the matched event (navy blue stars) moves away from the template event in both directions. Stations (triangles) are placed at three different epicentral distances ($R = 5, 50,$ or 150 km). The gray star marks the location of the matched event such that one of the stations (Sta3 in this case) is of equal distance to both the template and matched events. (b) For vertical interevent separation, the template event is placed at two different depths ($D = 3$ or 10 km) with the matched event moving up or down. (c, d) Correspond to a representative case with single-channel data, whereas (e) and (f) compile all test results with single-station (three-channel) data. Individual test results are presented in Figures S3 and S4. For (c) and (e), positive and negative horizontal separations indicate that the matched event is shifted to the south and north, respectively; for (d) and (f), positive and negative vertical separations indicate that the matched event is shifted down or up, respectively. CC, cross-correlation coefficient.

The degree of similarity can be expressed by the value of cross-correlation coefficient (CC) in the time domain or equivalently coherence in the frequency domain. The employed CC threshold is somewhat arbitrary, ranging from as low as 0.70 for regions with sparse network coverage to as high as 0.98 for areas with denser instrumentation (Table S1). The third way is a hybrid approach with complementary criteria in addition to CC (Table S1). The additional criteria differ significantly among various studies. Some studies examine the time interval between the event pair, the difference between the two event's S-P differential times, and/or the magnitude difference to minimize misidentification, while others directly verify the repeaters by relocating their hypocenters (Table S1).

With the increasing computing power, detecting repeaters through waveform similarity has become a routine process in seismology (e.g., Chamberlain et al., 2018, 2020; Tepp, 2018). However, a growing body of literature suggests that similar waveforms may only imply source proximity (Cheng et al., 2007; Ellsworth & Bulut, 2018) and/or similar focal mechanisms (Kilb & Rubin, 2002), but not necessarily repeating ruptures. One of the most striking examples is in central Japan where Cheng et al. (2007) analyze high-quality data from an extremely dense seismic array of 56 stations in a small area of $\sim 20 \times 20$ km and found no true repeaters among 807 very similar events ($CC \geq 0.80$). Their results highlight the serious reliability issue of using only waveform similarity in repeater identification.

The focus of this study, therefore, is to systematically investigate the deficiency of waveform similarity in repeater identification. We first examine how the CC varies with interevent separation and uncover the overlooked factors through a large number of synthetic experiments. We then illustrate that waveform similarity indeed lacks the resolution to determine whether two events are true repeaters or not using a dense local borehole array data in Parkfield, CA. To more reliably identify repeaters, we recommend the less popular physics-based approach that considers interevent overlap (e.g., Waldhauser & Ellsworth, 2002). We compare the effectiveness of the physics-based and waveform-similarity-based approaches using events occurred in the Fox Creek area, Alberta, Canada, where earthquake source parameters are well constrained by local stations.

2. Synthetic Experiments

Figure 1a illustrates the configuration of our synthetic experiments. We place one event (the template event) at the center of an array. Then, we incrementally shift the other event (the matched event) with the same focal mechanism in either north-south (Figure 1a) or vertical direction (Figure 1b). The technical details of our experiment setup and CC calculation are presented in the Supporting Information (Texts S1 and S2).

2.1. Constraining Interevent Separation Using Single-Channel Data

Single-channel CC has been used in numerous previous studies to infer the existence of repeaters (Table S1), thus we first examine how the CC varies with source separation using single-channel (i.e., E, N, or Z) data. In Figures 1c and 1d, we present the results of a representative case,

namely, a strike-slip earthquake (template event) at the depth of 3 km with a station 5 km away from the epicenter.

For horizontal interevent separation, our results indicate that single-channel waveforms can have very different sensitivities (Figure 1c). In general, the CC value decreases with increasing hypocentral separation. It quickly drops from 1 when the two sources are perfectly colocated to <0.5 when the pair is ~ 1 km apart. Beyond that, the CC curves appear to fluctuate between 0.2 and 0.4 without a clear monotonic trend. This implies that using the CC value to constrain the difference between two nearby hypocenters may not be ideal once the separation is on the order of kilometers.

Another important point in Figure 1c is that the CC value may be strongly affected by the combined effect of focal mechanism and relative position between the source and station. This effect is best illustrated by Station 3 as the interevent distance increases. For all three channels, the CC value decreases when the matched event shifts northward from 0 to -1.3 km. Once passing the -1.3 km mark, the CC value has a sudden drop on both E and Z channels but continues to increase on the N channel. This unexpected result happens when Station 3 is located very close to one of the assumed nodal planes (Figure 1a). As the matched event shifts northward, Station 3's position moves across the nodal plane and therefore causes polarity reversal on the Z and E channels. When the interevent separation reaches -2.6 km, Station 3 is nearly of equal distance to both the template and matched events (Figure 1a), leading to identical waveforms on the N channel but reversed shapes on the other two channels (Figure S1). Consequently, the final (maximum) CC values would be 1 for the N channel (taken when the two P-phases coincide) and ~ 0.5 – 0.6 for the Z and E channels (taken when the two P-phases are offset by half a cycle), even though the two events are 2.6 km apart. We have tested other types of focal mechanisms (pure normal or thrust-faulting) and the profound effect remains (Figure S2).

Unlike the cases of horizontal separation, the CC curves obtained with different channels and stations overall show similar trends when the two sources are vertically apart (Figure 1d), hinting that using the CC value to constrain the vertical interevent separation is probably independent of data channel and station azimuth. Especially for the vertical channel, stations with different azimuths can have identical sensitivities to the interevent separation when the focal mechanism is pure strike slip (Figure 1d, bottom panel). Notice that the CC curves derived from the E and N channels of Station 1 are identical to those from the N and E channels of Station 3, respectively (Figure 1d), due to the symmetrical station location on the focal sphere (Figure 1a). Results of these tests once again suggest that a smaller CC does not necessarily represent a larger separation once the vertical separation exceeds a certain threshold (~ 0.5 km). We also find that results from different focal mechanisms are comparable (Figure S2). Last but not the least, the CC value generally drops much faster with increasing vertical source separation (Figure 1c vs. Figure 1d) as a result of more minor discrepancies between waveforms. In other words, the CC seems to be much more sensitive to capture the vertical source shift than the horizontal.

The simple tests above demonstrate that, in addition to interevent distance, CC can be severely affected by the specific channel used, combined effect of focal mechanism and relative position between the source and station, and source separation direction (horizontal vs. vertical).

2.2. Constraining Interevent Separation Using Single-Station (Three-Channel) Data

If data from all three channels are included, we find that the CC sensitivity to source separation increases dramatically for the cases of horizontal separation (e.g., Figure 1c vs. Figure S3a) but insignificantly for those of vertical separation (e.g., Figure 1d vs. Figure S4a). For a given horizontal separation, Stations 1 and 3 tend to have the lowest and highest CC values, respectively (Figures 1e and S3). This is because the waveform discrepancies are more diagnostic in the direction approximately in line with the template and matched events, and vice versa. The results strongly suggest that station azimuth is an important factor that cannot be overlooked in single-station cases. In contrast, the influences of focal depth, epicentral distance, and source focal mechanisms seem to be limited (Figure S3).

The computed CC overall is very sensitive to vertical interevent separation with the only exception when the source is deep and the station is close (e.g., $D = 10$ km and $R = 5$ km, Figures 1f and S4). For a close station ($R = 5$ km) and a shallow source ($D = 3$ km), even a very small (0.2 km) vertical separation can lead

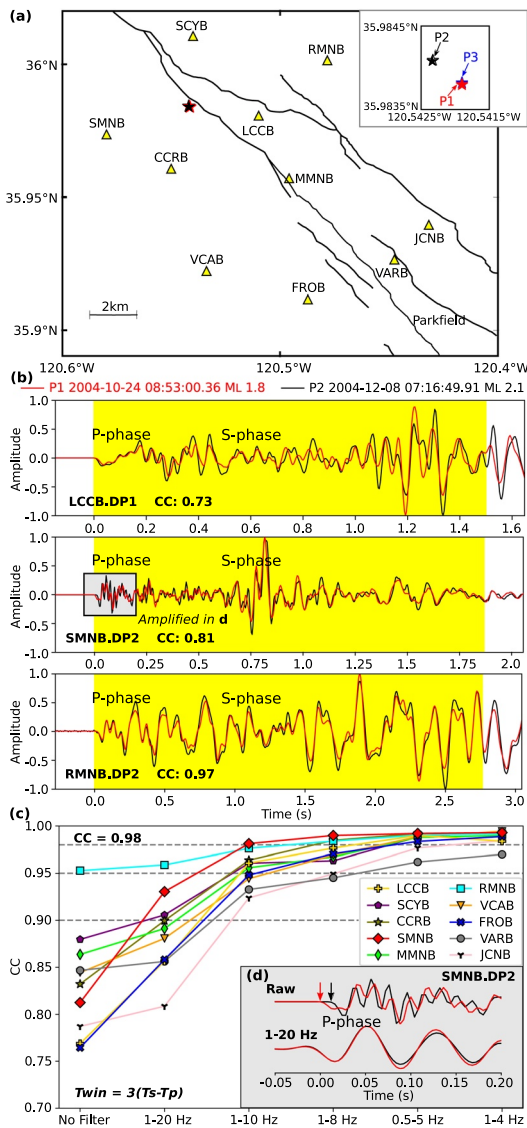


Figure 2. CC test results with real earthquake data from Parkfield, CA. (a) Map showing earthquake epicenters (colored stars; Waldhauser & Schaff, 2008) and HRSN seismograph stations (yellow triangles). Black lines denote known surface traces of the San Andreas Fault system. The green dot marks the town of Parkfield. Insert shows the zoom-in locations of events P1–3. (b) Normalized, unfiltered, and demeaned waveforms, aligned at the S-phase arrival. The highlighted segment indicates the window of dynamic length (see Text S2) used for CC calculation. The gray box in the middle panel outlines the waveform segment amplified in (d). (c) Effects of filtering on the CC values between the two events determined with individual single-station (three-channel) data and dynamic window lengths. (d) An example of waveform change due to filtering. Red and black arrows mark the P-phase onset of the two events. The slight time difference (0.012 s) between the two arrows is overlooked after band-pass filtering between 1 and 20 Hz. CC, cross-correlation coefficient; HRSN, High-Resolution Seismic Network.

to a dramatic drop of CC to <0.8 (Figures S4a and S4c), but the sensitivity gets worse when the source is deeper (Figures S4b and S4d). This is mainly a velocity structure effect caused by smaller seismic velocity variation at deep depths. In other words, the CC sensitivity would become higher when the corresponding velocity structure (and therefore the observed waveforms) is more complicated. An important observation to point out is that the CC is very sensitive to vertical interevent separations when the epicentral distance is large (e.g., $R = 50$ or 150 km), regardless of the focal depth (Figures S4e–S4l). This is opposite to what is expected for earthquake depth determination as seismic phase arrival times at distant stations usually have less depth constraint. It turns out that waveforms at distant stations can have better developed depth phases (i.e., seismic phases reflected from either the free surface or Moho). Consequently, a subtle change of source depth may lead to a significant waveform difference and hence an apparent CC drop. Therefore, our experiments in this section further demonstrate that CC can be affected by the number of channels used, station azimuth, velocity structure, and epicentral distance.

2.3. Constraining Interevent Separation Using Multistation Data

For areas with high station density (e.g., Japan), it is common to use a minimum of two stations (usually only the vertical channel) for identifying repeaters (Table S1). The majority of prior work (Table S1) calculate CC separately for each station. This approach essentially uses more stations with different azimuths and/or epicentral distances but may not necessarily improve the sensitivity if all available stations happen to be the ones with lower sensitivities (Figures 1e and 1f). An alternative way is to calculate the CC simultaneously across the network (2 out of 58 cases, Table S1) which includes the constraint of traveltime moveout. In such a case, the computed CC can be extremely sensitive to hypocenter difference (Gao & Kao, 2020). We refrain from investigating the multistation scenario as the CC sensitivity is known to be strongly affected by network geometry (Chamberlain & Townend, 2018; Gao & Kao, 2020), and thus no general/common rules can be inferred objectively.

In summary, our synthetic experiments reveal that CC is a very complex function of many aforementioned factors. A higher CC value does not necessarily represent a smaller interevent separation, and vice versa. Therefore, in contrast to the conventional wisdom, our synthetic results indicate that CC is not a robust indicator of two events being true repeaters or not.

3. Verification With Real Earthquake Examples

The High-Resolution Seismic Network (HRSN, Figure 2a) is a dense local array of borehole sensors deployed in the Parkfield area, CA, and operated by the Berkeley Seismological Laboratory. The HRSN waveform data primarily consist of seismic signals >1 Hz (instrument response shown in Figure S5) with an excellent signal-to-noise ratio (SNR) and a digitizing rate of 250 samples per second. Hence, this data set is ideal for the purpose of our study to verify whether waveform similarity is a

good proxy of repeater identification. Here, we take three events (P1–3, Figure 2a) from two well studied repeating earthquake clusters in Parkfield (e.g., Abercrombie, 2014; Dreger et al., 2007; Zoback et al., 2011).

Among them, events P1 and P3 belong to the same cluster with similar source areas while event P2 occurred on a neighboring fault patch.

3.1. CC Between Nonrepeaters

We first calculate the CC between neighboring events, that is, P1 and P2. We only use data from stations nearly free from noise contamination, as hinted by the flat waveforms before the *P* wave arrival (one example is shown in Figure 2b). The most striking result of our analysis is that the CC values derived from unfiltered three-channel waveforms indeed differ significantly among different stations, ranging from 0.76 to just above 0.95 (Figure 2c). Such a wide CC range is consistent with the inference from our synthetic tests that the CC can be severely affected by station azimuth and/or source–receiver position/path even under the extremely low noise circumstances. The relative deficiency of high-frequency signals in the waveforms of station RMNB (Figure 2b) may also contribute to the high CC of 0.95. This observation seems to suggest that site effect can affect the final CC result too. Additionally, the CC may be further affected by local structures of velocity discontinuities as this region is featured by complex fault zones (Figure 2a). Our study reveals that the waveforms of nonrepeaters can show apparent difference (top panel in Figure 2b), slight difference (middle panel in Figure 2b), or little difference (bottom panel in Figure 2b) at different stations. For any given station, the CC values of different channels can be either similar or different (Figure S6). Together, waveform similarity indeed lacks the resolution to decide if the two events are repeaters or not.

Because nearly all prior works practically identify repeaters through filtered waveforms for the purpose of mitigating the noise impact, we then examine the effects of commonly used band-pass filters (Table S2). Our results indicate that the CC obtained from different stations all show a clear increasing trend when the passband becomes narrower (Figures 2c and S6), consistent with the findings from synthetic experiments of an earlier study (Baisch et al., 2008). Especially for the very narrow but very popular 1–4 Hz band-pass filter used by many previous studies (Table S2), 9 out of 10 stations have $CC > 0.98$ (Figure 2c), which is the highest CC threshold used in the literature in selecting repeaters (Table S1). This simple experiment highlights the often-overlooked fact that filtering could remove the important frequency content in the signal that distinguishes the physical separation of the two events, in addition to reducing the unwanted noise. For example, even a very wide band-pass filter (1–20 Hz) would remove the very high-frequency signal with poor similarity and thus lead to very similar waveforms as shown in Figure 2d. What makes it worse is that filtering would change both the shape and width of the *P* wave and therefore make the subtle difference in the S–P differential traveltime (0.012 s in Figure 2d) unresolvable, effectively throwing away the most critical information on the interevent distance. Technically, resolving the 0.012 s time difference between the two P-phases would require the higher corner frequency of the applied band-pass filter to be at least 30 Hz, a scenario never considered by previous studies (Table S2). However, the small bias (0.012 s), equivalent to a mislocation of ~100 m (Hayward & Bostock, 2017), is sufficient to cause misinterpretation for events with small source dimension. The results here strongly imply that filtering would lead to misidentification of repeaters if the selection criterion is solely based on waveform similarity. We also tested the effect of template window length (T_{win}) associated with different filters (Table S2) in calculating CC (Text S2) and the results are comparable (Figure S7). Two examples of how filtering increases the waveform similarity at close and distant stations, respectively, are presented in Figures S8 and S9 for reference.

3.2. CC Between True Repeaters

Interestingly, we also find that, for true repeaters like events P1 and P3, the CC values obtained from different stations still differ significantly from each other (Figure S10). The unfiltered waveforms can be nearly identical at one station (Figure S11a) but have minor difference at another station even with extremely low noise (zoom-in box in Figure S11b). Without noise contamination, the waveform difference between true repeaters may arise from the variability of the rupture process (such as the slight difference in earthquake initiation point) (Uchida, 2019) and/or seismic velocity change (e.g., Pacheco et al., 2017; Poupinet et al., 1984). With the band-pass filters applied, the waveform discrepancy overall becomes much smaller as indicated by the increasing CC values (Figure S10). This is similar to, but less dramatic as, the case of nonrepeaters.

Taken together, nonrepeaters indeed can have very similar waveforms (bottom panel in Figure 2b) while the waveforms of true repeaters may display minor difference (Figure S11b). In contrast to the traditional view, our observations undoubtedly suggest that waveform similarity is not a good proxy for repeater identification, especially with band-pass filters applied.

4. Comparison Between Waveform-Similarity-Based and Physics-Based Approaches

The most fundamental concern of two events being repeaters or not is whether their ruptures significantly overlap with each other. However, there is no standard requirement about the minimum overlapping areas for repeater identification. Similar to the physical criterion adopted by some earlier studies (e.g., Waldhauser & Ellsworth, 2002; Zhao & Peng, 2008), we define two events to be repeaters if their interevent distance is no larger than the source dimension of the bigger event.

The rupture area of an earthquake can be measured directly from the corresponding slip distribution. In practice (especially for moderate and small events that can be approximated by point sources), however, the rupture area is commonly represented by the equivalent rupture radius (ERR, Table S3) that can be estimated from the corner frequency (f_c) of the P- or S-phase spectrum via the well-established circular dislocation model (Brune, 1970; Eshelby, 1957) as

$$\text{ERR} = \frac{kv}{f_c}, \quad (1)$$

where k is $1.6 / 2\pi$ for P waves and $1.99 / 2\pi$ for S waves, and v is the corresponding P- or S-phase velocity (Sato & Hirasawa, 1973).

Since the rupture radius of a circular fault is related to its scalar seismic moment (M_0) and stress drop ($\Delta\sigma$) as

$$\text{ERR} = \sqrt[3]{\frac{7M_0}{16\Delta\sigma}}, \quad (2)$$

many previous studies took this simplified approach by assuming a reasonable $\Delta\sigma$ value (Table S3). Because a smaller $\Delta\sigma$ value (or equivalently a smaller f_c) will yield a larger ERR, underestimation of $\Delta\sigma$ or f_c is likely to misclassify neighboring events as repeaters, and vice versa. Therefore, the uncertainty due to a poorly constrained (or wrongly assumed) $\Delta\sigma$ or f_c value should be treated with caution (Huang et al., 2020; L. Li et al., 2011). We note that ERR is the most popular, but not the only parameter. More precisely determined rupture distribution and/or geometry should be used to compare with the interevent distance for repeater identification whenever possible.

For the distance of interevent separation, however, it is always challenging to get a precise measurement unless a very dense local array is available (Cheng et al., 2007). In case of limited data, we propose a variant of the double-difference method (Waldhauser & Ellsworth, 2000) that minimizes the residual between observed and predicted relative S–P differential traveltime through three-dimensional grid search to precisely estimate the interevent distance. We explain the detail of our method, named the differential-traveltime double-difference (DTDD) method, in the Supporting Information (Text S3).

Figure 3 presents an example of using the DTDD method to determine the precise relative position of 12 events recorded at four nearby stations equipped with broadband sensors (instrument response shown in Figure S12 with a digitizing rate of 100 samples per second) in Fox Creek, Alberta, Canada. The ERRs (Table S4) of these events are well determined (Text S4). Among them, we identify two cases of repeating pairs (F3 and F4, and F2 and F6) that satisfy the condition of significantly overlapped source areas (i.e., $\text{ERR} > \text{interevent distance}$; Figure 3b). We note that the decision for event pair F7 and F9 can be ambiguous because the interevent distance is approximately the same as the ERR of event F9. It is, therefore, possible to qualify events F7 and F9 as repeaters if a different threshold is used. For the purpose of this demonstration, we decide to take a more conservative approach by considering only events without any controversy.

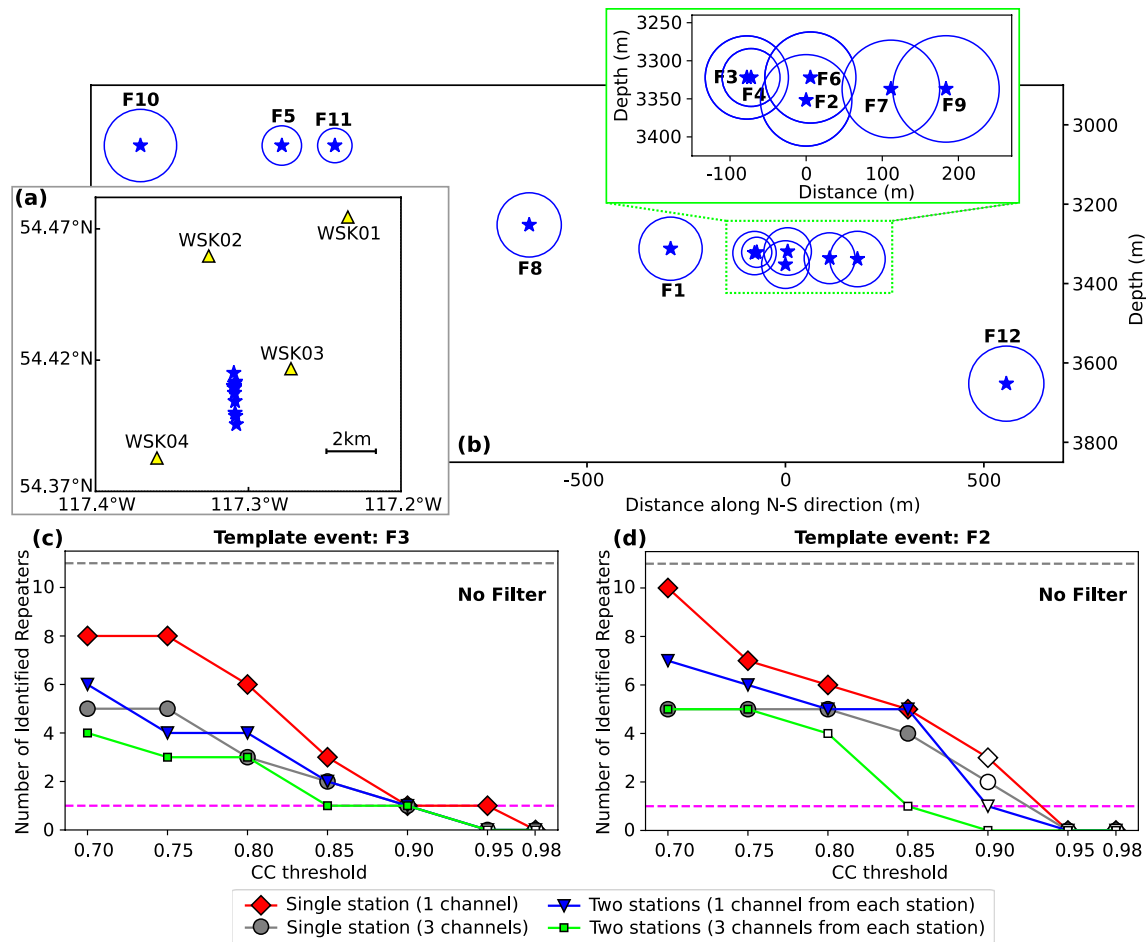


Figure 3. Comparison between waveform-similarity-based and physics-based approaches using earthquakes that occurred in Fox Creek, Alberta. (a) Map showing the distribution of earthquake epicenters (blue stars) and seismograph stations (yellow triangles). (b) N-S cross section of the earthquake sequence. Events are numbered chronologically and source parameters are provided in Table S4. Stars and circles represent the projected hypocenters and rupture areas, respectively. (c, d) Correspond to the number of identified repeaters using events F3 and F2 as the templates, respectively. Dashed gray and fuchsia lines depict the total number of events (11) and the number of true repeaters (1), respectively. Different symbols correspond to different data set. If the true repeater is not identified, open symbols are used instead.

We first use event F3 as the template to cross-correlate with the other 11 events. To investigate the inconsistency of the waveform-similarity-based identification approach, we systematically try a range of commonly used CC thresholds (Table S1), digital filters (Table S2), and data choices (single station with one channel, single station with three channels, two stations with one channel from each station, and two stations with three channels from each station, Table S1).

Figure 3c summarizes the results of misidentification using unfiltered waveforms. It is obvious that using data from more channels and/or stations can significantly minimize the chance of misidentification when the CC threshold is low (<0.90). Taking a CC threshold of 0.70 for example, using single-station (one channel) and two-station (six channels in total) data result in seven and three misidentifications, respectively. An increase in the CC threshold can dramatically reduce the misidentification ratio regardless of the data choice. However, the highest CC threshold does not necessarily lead to the correct answer. This is clear when we compare the results of setting the CC threshold to 0.90, 0.95, and 0.98. While a threshold of 0.90 can work perfectly for all cases, an extremely high threshold of 0.98 fails to recognize event F4 as a repeater of event F3.

When digital filters are applied, the misidentification rate is generally higher as the bandwidth narrows (Figure S13). In the worst-case scenario, all 10 nonrepeating events are misclassified as repeaters of event F3

when a CC threshold of ≤ 0.80 is chosen, a narrow band-pass (1–4 Hz) filter is applied, and only single-station (one channel) data are used (Figure S13e). Like the results with unfiltered waveforms, there are specific combinations of CC threshold, spectral passband, and data choice that can achieve 100% recall rate with zero misidentification. Unfortunately, no general rule can be derived (Figure S13).

To further validate our findings, we repeat the aforementioned analysis for the other repeating pair (events F2 and F6). Figures 3d and S14 show the results of using event F2 as the template. Despite all the combinations of CC threshold, spectral passband, and data choice, we cannot find any case with a perfect score. Our results underscore the challenge and risk in identifying repeaters solely based on waveform similarity.

5. Discussion and Conclusions

We have demonstrated that CC can be severely affected by many factors, including station azimuth, epicentral distance, velocity structure (including site effect), focal mechanism, network geometry, orientation of the source separation (horizontal vs. vertical), the choice of data (one specific channel or all three channels; one station or multiple stations), and the spectral passband used in data processing. Additionally, the level of background noise and the length of template waveforms may further influence the CC's sensitivity to interevent distance (Gao & Kao, 2020). One vivid example is the relocated aftershock distribution of the Mount Lewis (M_L 5.7) California earthquake that illuminate two faults with completely different orientations, even though all the relocated events have high waveform similarity (Kilb & Rubin, 2002). Therefore, we argue that it is extremely difficult, if not impossible, to reliably identify repeaters solely based on waveform similarity as the correct choice of all controlling parameters cannot be made beforehand (Table S5).

It is worth pointing out that nearly all previous waveform-similarity-based studies choose the CC threshold and the number of channels based on data availability and/or quality (Table S1), not the most accurate recovery rate. Similarly, the choice of spectral passband depends mostly on the event magnitude and/or noise characteristics (Table S2). Since no combinations of the selected CC threshold, data set, and digital filter can guarantee the accuracy of repeater identification, as demonstrated in Figures 2 and 3, we suggest that previously reported repeating earthquakes may be questionable if they are determined solely based on waveform similarity. A systematic reevaluation of previous identification results and their interpretations/hypotheses may be important and necessary.

In summary, robust identification of repeaters is very challenging. Our experiments systematically illustrate that waveform-similarity-based method lacks the resolution to distinguish repeating and neighboring events. In contrast, the physics-based approach is more reliable, but precise estimation of the interevent distance and source dimension for a large data set can be very labor intensive and time consuming (Table S5). An efficient solution is to use the waveform-similarity-based method as a preprocessor in the identification process (e.g., Cheng et al., 2007). We emphasize that choosing a proper filter is important for the optimal performance of waveform cross correlation (Gao & Kao, 2020). However, using unfiltered waveform data is necessary to maintain the correct time difference between P- and S-phases, which is crucial to repeater verification (e.g., L. Li et al., 2007, 2011). We also note that neither the waveform-similarity-based nor the physics-based approaches can work for data with a low SNR. Improving the quality of waveform data, therefore, can be the most effective way to correctly identify repeating earthquakes.

Data Availability Statement

The HRSN and Fox Creek event waveform data used in this study were downloaded from the Northern California Earthquake Data Center (NCEDC) (<http://ncedc.org/hrsn/>) and Incorporated Research Institutions for Seismology (IRIS) (<http://ds.iris.edu/ds/nodes/dmc/>), respectively. Seismic data are processed with Obspy (Beyreuther et al., 2010; <https://docs.obspy.org>). Figures are made with Matplotlib (Hunter, 2007; <https://matplotlib.org>) and Inkscape (<https://inkscape.org>).

Acknowledgments

We thank Editor Germán Prieto, Debi Kilb, and an anonymous reviewer for their constructive comments. We are grateful to Lupei Zhu for providing the FK code that is used in generating synthetic seismograms. We specially thank Didem Cambaz and Edwin Nissen for the help offered in this study. Insightful discussions with Stan Dasso, Toshihiro Igarashi, Naoki Uchida, David P. Schaff, Makoto Naoi, Jianlong Yuan, Kelin Wang, Ryan Visser, Rachel E. Abercrombie, Fengzhou Tan, Ramin Mohammad Hosseini Dokht, Wen-che Yu, Lingsen Meng, Hui Huang, Jean Schmittbuhl, Marco Bohnhoff, Christopher Wollin, Tomoaki Nishikawa, Emily Warren-Smith, Luis A. Dominguez, Tianhaozhe Sun, and Haipeng Luo are much appreciated. This study is partially supported by a University of Victoria Fellowship (DG), the Induced Seismicity Research Project of NRCan (HK), Geoscience BC (HK), and a NSERC Discovery Grant (HK). This paper is NRCan contribution 20210101.

References

- Abercrombie, R. E. (2014). Stress drops of repeating earthquakes on the San Andreas fault at Parkfield. *Geophysical Research Letters*, *41*, 8784–8791. <https://doi.org/10.1002/2014GL062079>
- Abercrombie, R. E., Chen, X., & Zhang, J. (2020). Repeating earthquakes with remarkably repeatable ruptures on the San Andreas fault at Parkfield. *Geophysical Research Letters*, *47*, e2020GL089820. <https://doi.org/10.1029/2020GL089820>
- Baisch, S., Ceranna, L., & Harjes, H. P. (2008). Earthquake cluster: What can we learn from waveform similarity? *Bulletin of the Seismological Society of America*, *98*(6), 2806–2814.
- Beyreuther, M., Barsch, R., Krischer, L., Megies, T., Behr, Y., & Wassermann, J. (2010). ObsPy: A Python toolbox for seismology. *Seismological Research Letters*, *81*(3), 530–533.
- Brune, J. N. (1970). Tectonic stress and the spectra of seismic shear waves from earthquakes. *Journal of Geophysical Research*, *75*(26), 4997–5009.
- Chamberlain, C. J., Hopp, C. J., Boese, C. M., Warren-Smith, E., Chambers, D., Chu, S. X., et al. (2018). EQcorrscan: Repeating and near-repeating earthquake detection and analysis in python. *Seismological Research Letters*, *89*(1), 173–181.
- Chamberlain, C. J., & Townend, J. (2018). Detecting real earthquakes using artificial earthquakes: On the use of synthetic waveforms in matched-filter earthquake detection. *Geophysical Research Letters*, *45*, 11641–11649. <https://doi.org/10.1029/2018GL079872>
- Chamberlain, C. J., Townend, J., & Gerstenberger, M. C. (2020). RT-EQcorrscan: Near-real-time matched-filtering for rapid development of dense earthquake catalogs. *Seismological Society of America*, *91*(6), 3574–3584.
- Cheng, X., Niu, F., Silver, P. G., Horiuchi, S., Takai, K., Iio, Y., & Ito, H. (2007). Similar microearthquakes observed in western Nagano, Japan, and implications for rupture mechanics. *Journal of Geophysical Research*, *112*, B04306. <https://doi.org/10.1029/2006JB004416>
- Dreger, D., Nadeau, R. M., & Chung, A. (2007). Repeating earthquake finite source models: Strong asperities revealed on the San Andreas Fault. *Geophysical Research Letters*, *34*, L23302. <https://doi.org/10.1029/2007GL031353>
- Ellsworth, W. L., & Bulut, F. (2018). Nucleation of the 1999 Izmit earthquake by a triggered cascade of foreshocks. *Nature Geoscience*, *11*(7), 531–535.
- Eshelby, J. D. (1957). The determination of the elastic field of an ellipsoidal inclusion, and related problems. *Proceedings of the Royal Society of London, Series A: Mathematical and Physical Sciences*, *241*(1226), 376–396.
- Gao, D., & Kao, H. (2020). Optimization of the match-filtering method for robust repeating earthquake detection: The multisegment cross-correlation approach. *Journal of Geophysical Research: Solid Earth*, *125*, e2020JB019714. <https://doi.org/10.1029/2020JB019714>
- Hatch, R. L., Abercrombie, R. E., Ruhl, C. J., & Smith, K. D. (2020). Evidence of aseismic and fluid-driven processes in a small complex seismic swarm near Virginia City, Nevada. *Geophysical Research Letters*, *47*, e2019GL085477. <https://doi.org/10.1029/2019GL085477>
- Hayward, T. W., & Bostock, M. G. (2017). Slip behavior of the queen Charlotte plate boundary before and after the 2012, M_w 7.8 Haida Gwaii earthquake: Evidence from repeating earthquakes. *Journal of Geophysical Research: Solid Earth*, *122*, 8990–9011. <https://doi.org/10.1002/2017JB014248>
- Huang, H., & Meng, L. (2018). Slow unlocking processes preceding the 2015 M_w 8.4 Illapel, Chile, earthquake. *Geophysical Research Letters*, *45*, 3914–3922. <https://doi.org/10.1029/2018GL077060>
- Huang, H., Meng, L., Bürgmann, R., Wang, W., & Wang, K. (2020). Spatio-temporal foreshock evolution of the 2019 M 6.4 and M 7.1 Ridgecrest, California earthquakes. *Earth and Planetary Science Letters*, *551*, 116582.
- Hunter, J. D. (2007). Matplotlib: A 2D graphics environment. *IEEE Annals of the History of Computing*, *9*(3), 90–95.
- Jiang, C., Wu, Z., Li, Y., & Ma, T. (2014). “Repeating events” as estimator of location precision: The China national seismograph network. *Pure and Applied Geophysics*, *171*(3–5), 413–423.
- Kato, A., & Nakagawa, S. (2014). Multiple slow-slip events during a foreshock sequence of the 2014 Iquique, Chile M_w 8.1 earthquake. *Geophysical Research Letters*, *41*, 5420–5427. <https://doi.org/10.1002/2014GL061138>
- Kato, A., Obara, K., Igarashi, T., Tsuruoka, H., Nakagawa, S., & Hirata, N. (2012). Propagation of slow slip leading up to the 2011 M_w 9.0 Tohoku-Oki earthquake. *Science*, *335*(6069), 705–708.
- Kilb, D., & Rubin, A. M. (2002). Implications of diverse fault orientations imaged in relocated aftershocks of the Mount Lewis, M_L 5.7, California, earthquake. *Journal of Geophysical Research*, *107*(B11), 2294. <https://doi.org/10.1029/2001JB000149>
- Li, A., & Richards, P. G. (2003). Using earthquake doublets to study inner core rotation and seismicity catalog precision. *Geochemistry, Geophysics, Geosystems*, *4*(9), 1072. <https://doi.org/10.1029/2002GC000379>
- Li, L., Chen, Q. F., Cheng, X., & Niu, F. (2007). Spatial clustering and repeating of seismic events observed along the 1976 Tangshan fault, north China. *Geophysical Research Letters*, *34*, L23309. <https://doi.org/10.1029/2007GL031594>
- Li, L., Chen, Q. F., Niu, F., & Su, J. (2011). Deep slip rates along the Longmen Shan fault zone estimated from repeating microearthquakes. *Journal of Geophysical Research*, *116*, B09310. <https://doi.org/10.1029/2011JB008406>
- Materna, K., Taira, T. A., & Bürgmann, R. (2018). Aseismic transform fault slip at the Mendocino triple junction from characteristically repeating earthquakes. *Geophysical Research Letters*, *45*, 699–707. <https://doi.org/10.1002/2017GL075899>
- Matsubara, M., Yagi, Y., & Obara, K. (2005). Plate boundary slip associated with the 2003 Off-Tokachi earthquake based on small repeating earthquake data. *Geophysical Research Letters*, *32*, L08316. <https://doi.org/10.1029/2004GL022310>
- Meier, T., Rische, M., Endrun, B., Vafidis, A., & Harjes, H. P. (2004). Seismicity of the Hellenic subduction zone in the area of western and central Crete observed by temporary local seismic networks. *Tectonophysics*, *383*(3–4), 149–169.
- Meng, L., Huang, H., Bürgmann, R., Ampuero, J. P., & Strader, A. (2015). Dual megathrust slip behaviors of the 2014 Iquique earthquake sequence. *Earth and Planetary Science Letters*, *411*, 177–187.
- Nadeau, R. M., & Johnson, L. R. (1998). Seismological studies at Parkfield VI: Moment release rates and estimates of source parameters for small repeating earthquakes. *Bulletin of the Seismological Society of America*, *88*(3), 790–814.
- Pacheco, K., Nishimura, T., & Nakahara, H. (2017). Seismic velocity changes of P and S waves associated with the 2011 Tohoku-Oki earthquake (M_w 9.0) as inferred from analyses of repeating earthquakes. *Geophysical Journal International*, *209*(1), 517–533.
- Poupinet, G., Ellsworth, W. L., & Frechet, J. (1984). Monitoring velocity variations in the crust using earthquake doublets: An application to the Calaveras Fault, California. *Journal of Geophysical Research*, *89*(B7), 5719–5731.
- Sato, T., & Hirasawa, T. (1973). Body wave spectra from propagating shear cracks. *Journal of Physics of the Earth*, *21*(4), 415–431.
- Sawazaki, K., Kimura, H., Shiomi, K., Uchida, N., Takagi, R., & Snieder, R. (2015). Depth-dependence of seismic velocity change associated with the 2011 Tohoku earthquake, Japan, revealed from repeating earthquake analysis and finite-difference wave propagation simulation. *Geophysical Journal International*, *201*(2), 741–763.
- Schaff, D. P., & Beroza, G. C. (2004). Coseismic and postseismic velocity changes measured by repeating earthquakes. *Journal of Geophysical Research*, *109*, B10302. <https://doi.org/10.1029/2004JB003011>

- Schaff, D. P., & Richards, P. G. (2011). On finding and using repeating seismic events in and near China. *Journal of Geophysical Research*, 116, B03309. <https://doi.org/10.1029/2010JB007895>
- Sheng, Y., Ellsworth, W. L., Lellouch, A., & Beroza, G. C. (2021). Depth constraints on coseismic velocity changes from frequency-dependent measurements of repeating earthquake waveforms. *Journal of Geophysical Research: Solid Earth*, 126, e2020JB020421. <https://doi.org/10.1029/2020JB020421>
- Tepp, G. (2018). A repeating event sequence alarm for monitoring volcanoes. *Seismological Research Letters*, 89(5), 1863–1876.
- Tkalčić, H., Young, M., Bodin, T., Ngo, S., & Sambridge, M. (2013). The shuffling rotation of the Earth's inner core revealed by earthquake doublets. *Nature Geoscience*, 6(6), 497–502.
- Uchida, N. (2019). Detection of repeating earthquakes and their application in characterizing slow fault slip. *Progress in Earth and Planetary Science*, 6(1), 40.
- Uchida, N., & Bürgmann, R. (2019). Repeating earthquakes. *Annual Review of Earth and Planetary Sciences*, 47, 305–332.
- Uchida, N., Matsuzawa, T., Hasegawa, A., & Igarashi, T. (2003). Interplate quasi-static slip off Sanriku, NE Japan, estimated from repeating earthquakes. *Geophysical Research Letters*, 30(15), 1801. <https://doi.org/10.1029/2003GL017452>
- Uchida, N., Matsuzawa, T., Hirahara, S., & Hasegawa, A. (2006). Small repeating earthquakes and interplate creep around the 2005 Miyagi-oki earthquake ($M = 7.2$). *Earth, Planets and Space*, 58(12), 1577–1580.
- Waldhauser, F., & Ellsworth, W. L. (2000). A double-difference earthquake location algorithm: Method and application to the northern Hayward fault, California. *Bulletin of the Seismological Society of America*, 90(6), 1353–1368.
- Waldhauser, F., & Ellsworth, W. L. (2002). Fault structure and mechanics of the Hayward fault, California, from double-difference earthquake locations. *Journal of Geophysical Research*, 107(B3), 2054. <https://doi.org/10.1029/2000JB000084>
- Waldhauser, F., & Schaff, D. P. (2008). Large-scale relocation of two decades of Northern California seismicity using cross-correlation and double-difference methods. *Journal of Geophysical Research*, 113, B08311. <https://doi.org/10.1029/2007JB005479>
- Wu, W., Zhan, Z., Peng, S., Ni, S., & Callies, J. (2020). Seismic ocean thermometry. *Science*, 369(6510), 1510–1515.
- Yamada, M., Mori, J., & Matsushi, Y. (2016). Possible stick-slip behavior before the Rausu landslide inferred from repeating seismic events. *Geophysical Research Letters*, 43, 9038–9044. <https://doi.org/10.1002/2016GL069288>
- Yu, W. C. (2013). Shallow-focus repeating earthquakes in the Tonga–Kermadec–Vanuatu subduction zones. *Bulletin of the Seismological Society of America*, 103(1), 463–486.
- Zhang, J., Richards, P. G., & Schaff, D. P. (2008). Wide-scale detection of earthquake waveform doublets and further evidence for inner core super-rotation. *Geophysical Journal International*, 174(3), 993–1006.
- Zhang, J., Song, X., Li, Y., Richards, P. G., Sun, X., & Waldhauser, F. (2005). Inner core differential motion confirmed by earthquake waveform doublets. *Science*, 309(5739), 1357–1360.
- Zhao, P., & Peng, Z. (2008). Velocity contrast along the Calaveras fault from analysis of fault zone head waves generated by repeating earthquakes. *Geophysical Research Letters*, 35, L01303. <https://doi.org/10.1029/2007GL031810>
- Zoback, M., Hickman, S., & Ellsworth, W. (2011). Scientific drilling into the San Andreas fault zone—An overview of SAFOD's first five years. *Scientific Drilling*, 11, 14–28.

References From the Supporting Information

- Abercrombie, R. E., Poli, P., & Bannister, S. (2017). Earthquake directivity, orientation, and stress drop within the subducting plate at the Hikurangi Margin, New Zealand. *Journal of Geophysical Research: Solid Earth*, 122, 10176–10188. <https://doi.org/10.1002/2017JB014935>
- Bao, X., & Eaton, D. W. (2016). Fault activation by hydraulic fracturing in western Canada. *Science*, 354(6318), 1406–1409.
- Bohnhoff, M., Wollin, C., Domigall, D., Küperkoch, L., Martínez-Garzón, P., Kwiatak, G., et al. (2017). Repeating Marmara Sea earthquakes: Indication for fault creep. *Geophysical Journal International*, 210(1), 332–339.
- Bruce, J. N. (1971). Correction to tectonic stress and the spectra of seismic shear waves from earthquakes. *Journal of Geophysical Research*, 76(20), 5002.
- Buurman, H., & West, M. E. (2010). Seismic precursors to volcanic explosions during the 2006 eruption of Augustine Volcano. In J. A. Power, M. L. Coombs, & J. T. Freymueller (Eds.), *The 2006 eruption of Augustine volcano, Alaska, Professional paper* (Vol. 1769, pp. 41–57). Washington, DC: U.S. Geological Survey.
- Buurman, H., West, M. E., & Thompson, G. (2013). The seismicity of the 2009 Redoubt eruption. *Journal of Volcanology and Geothermal Research*, 259, 16–30.
- Cannata, A., Alparone, S., & Ursino, A. (2013). Repeating volcano-tectonic earthquakes at Mt. Etna volcano (Sicily, Italy) during 1999–2009. *Gondwana Research*, 24(3–4), 1223–1236.
- Cauchie, L., Lengliné, O., & Schmittbuhl, J. (2020). Seismic asperity size evolution during fluid injection: Case study of the 1993 Soultz-sous-Forêts injection. *Geophysical Journal International*, 221(2), 968–980.
- Chaves, E. J., Schwartz, S. Y., & Abercrombie, R. E. (2020). Repeating earthquakes record fault weakening and healing in areas of megathrust postseismic slip. *Science Advances*, 6(32), eaaz9317.
- Chen, K. H., Nadeau, R. M., & Rau, R. J. (2008). Characteristic repeating earthquakes in an arc-continent collision boundary zone: The Chihshang fault of eastern Taiwan. *Earth and Planetary Science Letters*, 276(3–4), 262–272.
- Cociani, L., Bean, C. J., Lyon-Caen, H., Pacchiani, F., & Deschamps, A. (2010). Coseismic velocity variations caused by static stress changes associated with the 2001 $M_w = 4.3$ Agios Ioanis earthquake in the Gulf of Corinth, Greece. *Journal of Geophysical Research*, 115, B07313. <https://doi.org/10.1029/2009JB006859>
- De Angelis, S., & Henton, S. M. (2011). On the feasibility of magma fracture within volcanic conduits: Constraints from earthquake data and empirical modeling of magma viscosity. *Geophysical Research Letters*, 38, L19310. <https://doi.org/10.1029/2011GL049297>
- Dominguez, L. A., Taira, T. A., & Santoyo, M. A. (2016). Spatiotemporal variations of characteristic repeating earthquake sequences along the Middle America Trench in Mexico. *Journal of Geophysical Research: Solid Earth*, 121, 8855–8870. <https://doi.org/10.1002/2016JB013242>
- Eaton, D. W., Igonin, N., Poulin, A., Weir, R., Zhang, H., Pellegrino, S., & Rodriguez, G. (2018). Induced seismicity characterization during hydraulic-fracture monitoring with a shallow-wellbore geophone array and broadband sensors. *Seismological Research Letters*, 89(5), 1641–1651.
- Green, D. N., & Neuberg, J. (2006). Waveform classification of volcanic low-frequency earthquake swarms and its implication at Soufrière Hills Volcano, Montserrat. *Journal of Volcanology and Geothermal Research*, 153(1–2), 51–63.

- Harrington, R. M., & Brodsky, E. E. (2009). Source duration scales with magnitude differently for earthquakes on the San Andreas Fault and on secondary faults in Parkfield, California. *Bulletin of the Seismological Society of America*, 99(4), 2323–2334.
- Hatakeyama, N., Uchida, N., Matsuzawa, T., & Nakamura, W. (2017). Emergence and disappearance of interplate repeating earthquakes following the 2011 Mw 9.0 Tohoku-oki earthquake: Slip behavior transition between seismic and aseismic depending on the loading rate. *Journal of Geophysical Research: Solid Earth*, 122, 5160–5180. <https://doi.org/10.1002/2016JB013914>
- Huang, Y., Beroza, G. C., & Ellsworth, W. L. (2016). Stress drop estimates of potentially induced earthquakes in the Guy-Greenbrier sequence. *Journal of Geophysical Research: Solid Earth*, 121, 6597–6607. <https://doi.org/10.1002/2016JB013067>
- Igarashi, T. (2010). Spatial changes of inter-plate coupling inferred from sequences of small repeating earthquakes in Japan. *Geophysical Research Letters*, 37, L20304. <https://doi.org/10.1029/2010GL044609>
- Igarashi, T. (2020). Catalog of small repeating earthquakes for the Japanese Islands. *Earth, Planets and Space*, 72, 1–8.
- Igarashi, T., Matsuzawa, T., & Hasegawa, A. (2003). Repeating earthquakes and interplate aseismic slip in the northeastern Japan subduction zone. *Journal of Geophysical Research*, 108(B5), 2249. <https://doi.org/10.1029/2002JB001920>
- Kato, A., & Igarashi, T. (2012). Regional extent of the large coseismic slip zone of the 2011 Mw 9.0 Tohoku-Oki earthquake delineated by on-fault aftershocks. *Geophysical Research Letters*, 39, L15301. <https://doi.org/10.1029/2012GL052220>
- Kimura, H., Kasahara, K., Igarashi, T., & Hirata, N. (2006). Repeating earthquake activities associated with the Philippine Sea plate subduction in the Kanto district, central Japan: A new plate configuration revealed by interplate aseismic slips. *Tectonophysics*, 417(1–2), 101–118.
- Kraft, T., & Deichmann, N. (2014). High-precision relocation and focal mechanism of the injection-induced seismicity at the Basel EGS. *Geothermics*, 52, 59–73.
- Lengliné, O., & Marsan, D. (2009). Inferring the coseismic and postseismic stress changes caused by the 2004 Mw = 6 Parkfield earthquake from variations of recurrence times of microearthquakes. *Journal of Geophysical Research*, 114, B10303. <https://doi.org/10.1029/2008JB006118>
- Li, L., Niu, F., Chen, Q. F., Su, J., & He, J. (2017). Post-seismic velocity changes along the 2008 M 7.9 Wenchuan earthquake rupture zone revealed by S coda of repeating events. *Geophysical Journal International*, 208(2), 1237–1249.
- Ma, S. (2010). Focal depth determination for moderate and small earthquakes by modeling regional depth phases sPg, sPmP, and sPn. *Bulletin of the Seismological Society of America*, 100(3), 1073–1088.
- Ma, S., & Atkinson, G. M. (2006). Focal depths for small to moderate earthquakes ($mN \geq 2.8$) in Western Quebec, Southern Ontario, and Northern New York. *Bulletin of the Seismological Society of America*, 96(2), 609–623.
- Ma, X., Wu, Z., & Jiang, C. (2014). ‘Repeating earthquakes’ associated with the WFS-1 drilling site. *Tectonophysics*, 619, 44–50.
- Ma, X. J., & Wu, Z. L. (2013). ‘Negative repeating doublets’ in an aftershock sequence. *Earth, Planets and Space*, 65(8), 923–927.
- Matsuzawa, T., Uchida, N., Igarashi, T., Okada, T., & Hasegawa, A. (2004). Repeating earthquakes and quasi-static slip on the plate boundary east off northern Honshu, Japan. *Earth, Planets and Space*, 56(8), 803–811.
- Mesimeri, M., & Karakostas, V. (2018). Repeating earthquakes in western Corinth Gulf (Greece): Implications for aseismic slip near locked faults. *Geophysical Journal International*, 215(1), 659–676.
- Myhill, R., McKenzie, D., & Priestley, K. (2011). The distribution of earthquake multiplets beneath the southwest Pacific. *Earth and Planetary Science Letters*, 301(1–2), 87–97.
- Nadeau, R. M., Foxall, W., & McEvilly, T. V. (1995). Clustering and periodic recurrence of microearthquakes on the San Andreas fault at Parkfield, California. *Science*, 267(5197), 503–507.
- Nadeau, R. M., & McEvilly, T. V. (1999). Fault slip rates at depth from recurrence intervals of repeating microearthquakes. *Science*, 285(5428), 718–721.
- Nadeau, R. M., & McEvilly, T. V. (2004). Periodic pulsing of characteristic microearthquakes on the San Andreas fault. *Science*, 303(5655), 220–222.
- Naoui, M., Nakatani, M., Igarashi, T., Otsuki, K., Yabe, Y., Kgarume, T., et al. (2015). Unexpectedly frequent occurrence of very small repeating earthquakes ($-5.1 \leq MW \leq -3.6$) in a South African gold mine: Implications for monitoring intraplate faults. *Journal of Geophysical Research: Solid Earth*, 120, 8478–8493. <https://doi.org/10.1002/2015JB012447>
- Nishikawa, T., & Ide, S. (2018). Recurring slow slip events and earthquake nucleation in the source region of the M7 Ibaraki-Oki earthquakes revealed by earthquake swarm and foreshock activity. *Journal of Geophysical Research: Solid Earth*, 123, 7950–7968. <https://doi.org/10.1029/2018JB015642>
- Obana, K., Kodaira, S., Kaneda, Y., Mochizuki, K., Shinohara, M., & Suyehiro, K. (2003). Microseismicity at the seaward updip limit of the western Nankai Trough seismogenic zone. *Journal of Geophysical Research*, 108(B10), 2459. <https://doi.org/10.1029/2002JB002370>
- Peng, Z., & Ben-Zion, Y. (2005). Spatiotemporal variations of crustal anisotropy from similar events in aftershocks of the 1999 M7.4 Izmit and M7.1 Düzce, Turkey, earthquake sequences. *Geophysical Journal International*, 160(3), 1027–1043.
- Petersen, T. (2007). Swarms of repeating long-period earthquakes at Shishaldin Volcano, Alaska, 2001–2004. *Journal of Volcanology and Geothermal Research*, 166(3–4), 177–192.
- Rau, R. J., Chen, K. H., & Ching, K. E. (2007). Repeating earthquakes and seismic potential along the northern Longitudinal Valley fault of eastern Taiwan. *Geophysical Research Letters*, 34, L24301. <https://doi.org/10.1029/2007GL031622>
- Robinson, D. J., Sambridge, M., & Snieder, R. (2011). A probabilistic approach for estimating the separation between a pair of earthquakes directly from their coda waves. *Journal of Geophysical Research*, 116, B04309. <https://doi.org/10.1029/2010JB007745>
- Salvage, R. O., & Neuberg, J. W. (2016). Using a cross correlation technique to refine the accuracy of the Failure Forecast Method: Application to Soufrière Hills volcano, Montserrat. *Journal of Volcanology and Geothermal Research*, 324, 118–133.
- Schmittbuhl, J., Karabulut, H., Lengliné, O., & Bouchon, M. (2016). Long-lasting seismic repeaters in the Central basin of the Main Marmara fault. *Geophysical Research Letters*, 43, 9527–9534. <https://doi.org/10.1002/2016GL070505>
- Schultz, R., Stern, V., & Gu, Y. J. (2014). An investigation of seismicity clustered near the Cordell Field, west central Alberta, and its relation to a nearby disposal well. *Journal of Geophysical Research: Solid Earth*, 119, 3410–3423. <https://doi.org/10.1002/2013JB010836>
- Schultz, R., Wang, R., Gu, Y. J., Haug, K., & Atkinson, G. (2017). A seismological overview of the induced earthquakes in the Duvernay play near Fox Creek, Alberta. *Journal of Geophysical Research: Solid Earth*, 122, 492–505. <https://doi.org/10.1002/2016JB013570>
- Shearer, P. M. (1997). Improving local earthquake locations using the L1 norm and waveform cross correlation: Application to the Whittier Narrows, California, aftershock sequence. *Journal of Geophysical Research*, 102(B4), 8269–8283.
- Shearer, P. M. (2009). *Introduction to seismology*. Cambridge: Cambridge University Press.
- Shearer, P. M., Abercrombie, R. E., Trugman, D. T., & Wang, W. (2019). Comparing EGF methods for estimating corner frequency and stress drop from P wave spectra. *Journal of Geophysical Research: Solid Earth*, 124, 3966–3986. <https://doi.org/10.1029/2018JB016957>

- Shirzaei, M., Bürgmann, R., & Taira, T. A. (2013). Implications of recent asperity failures and aseismic creep for time-dependent earthquake hazard on the Hayward fault. *Earth and Planetary Science Letters*, *371*, 59–66.
- Snieder, R., & Vrijlandt, M. (2005). Constraining the source separation with coda wave interferometry: Theory and application to earthquake doublets in the Hayward fault, California. *Journal of Geophysical Research*, *110*, B04301. <https://doi.org/10.1029/2004JB003317>
- Taira, T. A., Bürgmann, R., Nadeau, R. M., & Dreger, D. S. (2014). Variability of fault slip behavior along the San Andreas Fault in the San Juan Bautista Region. *Journal of Geophysical Research: Solid Earth*, *119*, 8827–8844. <https://doi.org/10.1002/2014JB011427>
- Thelen, W., Malone, S., & West, M. (2011). Multiplets: Their behavior and utility at dacitic and andesitic volcanic centers. *Journal of Geophysical Research*, *116*, B08210. <https://doi.org/10.1029/2010JB007924>
- Thelen, W., West, M., & Senyukov, S. (2010). Seismic characterization of the fall 2007 eruptive sequence at Bezymianny Volcano, Russia. *Journal of Volcanology and Geothermal Research*, *194*(4), 201–213.
- Trugman, D. T., & Shearer, P. M. (2017). GrowClust: A hierarchical clustering algorithm for relative earthquake relocation, with application to the Spanish Springs and Sheldon, Nevada, earthquake sequences. *Seismological Research Letters*, *88*(2A), 379–391.
- Uchida, N., & Matsuzawa, T. (2013). Pre- and postseismic slow slip surrounding the 2011 Tohoku-oki earthquake rupture. *Earth and Planetary Science Letters*, *374*, 81–91.
- Viegas, G., Abercrombie, R. E., & Kim, W. Y. (2010). The 2002 M5 Au Sable Forks, NY, earthquake sequence: Source scaling relationships and energy budget. *Journal of Geophysical Research*, *115*, B07310. <https://doi.org/10.1029/2009JB006799>
- Wang, B., Harrington, R. M., Liu, Y., Kao, H., & Yu, H. (2020). A study on the largest hydraulic-fracturing-induced earthquake in Canada: Observations and static stress-drop estimation. *Bulletin of the Seismological Society of America*, *110*(5), 2283–2294.
- Wang, R., Gu, Y. J., Schultz, R., Zhang, M., & Kim, A. (2017). Source characteristics and geological implications of the January 2016 induced earthquake swarm near Crooked Lake, Alberta. *Geophysical Journal International*, *210*(2), 979–988.
- Warren-Smith, E., Chamberlain, C. J., Lamb, S., & Townend, J. (2017). High-precision analysis of an aftershock sequence using matched-filter detection: The 4 May 2015 ML 6 Wanaka earthquake, Southern Alps, New Zealand. *Seismological Research Letters*, *88*(4), 1065–1077.
- Warren-Smith, E., Fry, B., Kaneko, Y., & Chamberlain, C. J. (2018). Foreshocks and delayed triggering of the 2016 MW 7.1 Te Araroa earthquake and dynamic reinvigoration of its aftershock sequence by the MW 7.8 Kaikōura earthquake, New Zealand. *Earth and Planetary Science Letters*, *482*, 265–276.
- Yamaguchi, J., Naoi, M., Nakatani, M., Moriya, H., Igarashi, T., Murakami, O., et al. (2018). Emergence and disappearance of very small repeating earthquakes on a geological fault in a gold mine in South Africa. *Tectonophysics*, *747*, 318–326.
- Yamashita, Y., Shimizu, H., & Goto, K. (2012). Small repeating earthquake activity, interplate quasi-static slip, and interplate coupling in the Hyuga-nada, southwestern Japan subduction zone. *Geophysical Research Letters*, *39*, L08304. <https://doi.org/10.1029/2012GL051476>
- Yao, D., Walter, J. I., Meng, X., Hobbs, T. E., Peng, Z., Newman, A. V., et al. (2017). Detailed spatiotemporal evolution of microseismicity and repeating earthquakes following the 2012 Mw 7.6 Nicoya earthquake. *Journal of Geophysical Research: Solid Earth*, *122*, 524–542. <https://doi.org/10.1002/2016JB013632>
- Zhao, P., & Peng, Z. (2009). Depth extent of damage zones around the central Calaveras fault from waveform analysis of repeating earthquakes. *Geophysical Journal International*, *179*(3), 1817–1830.
- Zhu, L., & Rivera, L. A. (2002). A note on the dynamic and static displacements from a point source in multilayered media. *Geophysical Journal International*, *148*(3), 619–627.